The Stabilizing Effect of a Hybrid Surface Coating on Ni-rich NCM Cathode Material in All-Solid-State Batteries

A-Young Kim,[†,*] Florian Strauss,[†,*] Timo Bartsch,[†] Jun Hao Teo,[†] Toru Hatsukade,[†] Andrey Mazilkin,[†,‡] Jürgen Janek,[†,#] Pascal Hartmann,[†,§] and Torsten Brezesinski[†,*]

[†] Battery and Electrochemistry Laboratory, Institute of Nanotechnology, Karlsruhe Institute of Technology (KIT), Hermann-von-Helmholtz-Platz 1, 76344 Eggenstein-Leopoldshafen, Germany.

[‡] Institute of Solid State Physics, Russian Academy of Sciences, Ac. Ossipyan str. 2, 142432 Chernogolovka, Russia.

[#] Institute of Physical Chemistry & Center for Materials Science, Justus-Liebig-University Giessen, Heinrich-Buff-Ring 17, 35392 Giessen, Germany.

[§] BASF SE, Carl-Bosch-Strasse 38, 67056 Ludwigshafen, Germany.

TOC Graphic

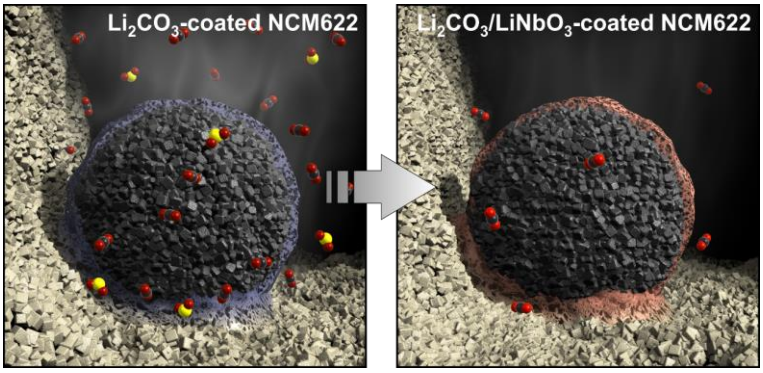

Abstract

Bulk-type all-solid-state batteries (SSBs) are receiving much attention as next-generation energy storage technology with potentially improved safety and higher power and energy densities (over a wider operating temperature range) compared to conventional Li-ion batteries (LIBs). However, practical implementation of SSBs faces a number of hurdles, such as issues related to interfacial stability between the solid electrolyte and the other active and inactive electrode constituents. One approach to effectively prevent or mitigate side reactions at the positive electrode is through surface coating of the cathode material with a dielectric material. In this article, we report on the preparation of Li_2CO_3- and Li_2CO_3/$LiNbO_3$-coated NCM622 (60% Ni) for application in pelletized SSB cells using β-Li_3PS_4 as solid electrolyte. Specifically, we demonstrate that in contrast to state-of-the-art LIBs, the presence of surface carbonate contaminants helps to improve the cell cyclability and the combination of carbonate and niobate species in a kind of hybrid or solid solution coating is particularly beneficial for achieving stable performance of Ni-rich NCM composite cathodes of practical loading (91% capacity retention after 100 cycles at a C/10 rate and 25 °C). This is due in part to the formation of robust interfaces in the cathode layer, strongly suppressing CO_2 evolution, due to decomposition of the relevant carbonate species, and accompanied SO_2 formation and release during cycling operation.

Introduction

With the growing use of liquid electrolyte-based Li-ion batteries (LIBs), especially for electric vehicles, the need for even higher power and energy density devices is increasing.[1–3] In this regard, all-solid-state batteries (SSBs) are being considered a promising next-generation energy storage technology.[4] Bulk-type SSBs can be realized by application of Ni-rich layered oxide ($LiNi_{1-x-y}Co_xMn_yO_2$, referred to as NCM or NMC) cathode active materials (CAMs) and lithium thiophosphate solid electrolytes (SEs), for example.[5] However, lithium thiophosphates suffer from decomposition reactions at the interfaces during cycling (due to stability issues), leading to poor reversibility and fast capacity fade.[6] Consequently, it seems indispensable to apply a protective coating to the CAM particles to prevent detrimental side reactions. Ideally, such surface layer should be stable against electrochemical oxidation while exhibiting high Li-ion conductivity and very low electronic conductivity.[7–9]

In recent years, various lithium metal oxides such as $Li_4Ti_5O_{12}$,[8] $LiNbO_3$,[10] $LiTaO_3$,[11] $LiAlO_2$,[12] and Li_2ZrO_3[13,14] have been tested as potential coating materials. Of note, lithium phosphate (Li_3PO_4),[15] borate (Li_3BO_3),[16] silicate (Li_2SiO_3),[17] and carbonate (Li_2CO_3)[18,19] have been studied as well. Among them, $LiNbO_3$ turned out to be one of the best performing coating materials due to its relatively high ionic conductivity and low electronic conductivity when in an amorphous state.[20] Applying such amorphous coating to Ni-rich layered oxide CAMs effectively inhibits interfacial SE decomposition, allowing for relatively stable cell operation.[21] Moreover, it is known that Ni-rich NCM shows a strong tendency for surface “impurity” formation when exposed to ambient atmosphere conditions.[22,23] These surface contaminants negatively affect the electrochemical performance, and especially Li_2CO_3 can cause gas evolution in both

liquid electrolyte-based LIBs and SSB cells.[24–26] Nonetheless, artificially grown Li_2CO_3 may act as a protective surface coating.[18,19] Interestingly, the surface contaminants can also be incorporated into the coating layer, thereby improving the cycling performance.[16,27]

In an effort to increase the Li-ion conductivity of ternary lithium metal oxide coatings, a mixture of borate and carbonate has been reported to exhibit properties better than those of the individual base materials.[16] Having this in mind, we embarked in the investigation of a Li_2CO_3/$LiNbO_3$ hybrid coating on NCM622 (60% Ni). $LiNbO_3$ was chosen in the present work, because it has already proven an effective coating material in the SSB area. Note that the synthesis protocol typically involves calcination with oxygen/air at moderate temperatures. However, the intrinsic tendency of Ni-rich CAMs to readily form Li_2CO_3 during surface treatment and subsequent processing has not been considered in the past. We show that the combination of carbonate and niobate species in the coating layer significantly improves the capacity retention of SSB cells using β-Li_3PS_4 SE. This result can be explained by the formation of more stable SE/CAM interfaces compared to that achieved with only Li_2CO_3-coated NCM622. Taken together, our research data demonstrate the positive effect of a novel hybrid or solid solution surface coating on the cycling behavior of Ni-rich layered oxide cathodes in bulk-type SSB cells.

Experimental

Materials

NCM622 powder (BASF SE; d_{50} = 2.9 µm, d_{90} = 6.0 µm) was dried for 12 h in vacuum at 300 °C and then stored in an Ar-filled glovebox (MBraun; [O_2], [H_2O] < 0.1 ppm).[28,29] 1 M lithium ethoxide solution was prepared by reacting absolute ethanol (Sigma-Aldrich; 99.8%) and Li metal (Albemarle Germany GmbH). For 0.5 M niobium ethoxide solution, $Nb(OCH_2CH_3)_5$ (Sigma-Aldrich; 99.95%) was dissolved in absolute ethanol.

Li_2CO_3/$LiNbO_3$ Layer Formation on NCM622

For the preparation of 1 wt.% Li_2CO_3/$LiNbO_3$-coated NCM622, CAM powder (5.94 g) was added to a mixture of lithium ethoxide (406 µL) and niobium ethoxide solutions (812 µL) in an Ar-filled glovebox, followed by sonication for 30 min in an ultrasonic bath. Subsequently, the reaction mixture was dried in vacuum until the solvent completely evaporated. The resultant powder was ground using mortar and pestle and calcined in air at 300 °C for 2 h (5 °C min^{-1} heating rate). For comparison, Li_2CO_3-coated NCM622 was prepared by the same procedure, but without using the Nb precursor.

Preparation of Electrode Composites

Cathode composite powder was prepared by milling NCM622 and β-Li_3PS_4 (BASF SE; 1 g, 7/3 weight ratio) using 10 zirconia balls (Ø 10 mm) in a planetary mill at 140 rpm for 30 min under an Ar atmosphere. Anode composite powder was a 3/6/1 weight ratio mixture of carbon-coated $Li_4Ti_5O_{12}$ (BASF SE; LTO), β-Li_3PS_4, and Super C65 carbon black (Timcal), and it was prepared by the same milling procedure as described before.

Cell Assembly and Electrochemical Testing

A custom setup was used for testing of the SSB cells (Ø 10 mm).[30] In the assembling procedure, β-Li_3PS_4 SE (60 mg) was compressed at 125 MPa (~500 µm thickness). Then, anode composite (30 mg, ~2.0 mAh cm^{-2}) was pressed to the SE pellet at 125 MPa (~120 µm thickness) and finally cathode composite (10-12 mg, 1.6-1.9 mAh cm^{-2}) was pressed onto the other side at 375 MPa (~90 µm thickness). During electrochemical testing, a pressure of 55 MPa was maintained. Galvanostatic measurements were performed at a C/10 rate (1C = 180 mA g_{NCM}^{-1}) and 25 °C in the voltage range between 1.35 and 2.85 V vs $Li_4Ti_5O_{12}/Li_7Ti_5O_{12}$ (equivalent to ~2.9-4.4 V vs Li^+/Li) using a MACCOR battery test system.

Electrochemical impedance spectroscopy (EIS) was performed using a VMP3 multi-channel potentiostat (BioLogic). The spectra were collected in the frequency range between 100 mHz and 7 MHz applying an AC voltage of 7 mV. Experimental data were fitted using a (R_1/Q_1)-(R_2/Q_2)-(R_3/Q_3)-Q_4 equivalent circuit, corresponding to $R_{SE\ bulk}$, $R_{SE\ grain\ boundary}$, interfacial $R_{SE/CAM}$, and Warburg impedance, respectively.[6,8,12]

Characterization

Scanning electron microscopy (SEM) and energy-dispersive X-ray spectroscopy (EDX) were performed using a LEO-1530 microscope (Carl Zeiss AG) with field emission source at 10 and 20 kV, respectively.

Transmission electron microscopy (TEM) was performed on a Titan 80-300 microscope (FEI Company). To protect the surface coating from damage during sample preparation and processing, Pt layers were deposited by electron beam and ion beam-induced deposition (FEI Strata).

The phase composition of as-synthesized materials was examined by powder X-ray diffraction (PXRD) using a Bruker D8 Advance diffractometer equipped with a Cu-Kα radiation source and a LYNXEYE 1D detector. PXRD patterns were collected in the 2θ range of 10-70° with a step size of 0.012° and an exposure time of 20 s per step.

Attenuated total reflection-infrared spectroscopy (ATR-IR) was performed on an ALPHA FT-IR spectrometer (Bruker) equipped with a Ge crystal in an Ar-filled glovebox. The spectra were collected using the OPUS software.

To quantify the amount of surface carbonate on NCM622, acid titration coupled with mass spectrometry was performed. The setup used consists of a septum-sealed vial containing the cathode material, a mass spectrometer (Pfeiffer Vacuum GmbH; HiCube Pro with PrismaPlus detector), and a mass flow controller (Bronkhorst; F-201CV-020-RAD-22-Z). The flow rate of Ar carrier gas was controlled at 2.5 mL min^{-1}. 1 M H_2SO_4 was injected into the vial using a needle. 10 mg CAM powder was exposed to about 0.35 mL H_2SO_4. For quantification, calibration gas was passed through the system after each run.

The niobium and transition-metal contents were determined via inductively coupled plasma optical emission spectroscopy (ICP-OES) on both a PerkinElmer Optima 4300 DV and a Thermo Scientific iCAP 7600.

X-ray photoelectron spectroscopy (XPS) was performed on a K-Alpha XPS spectrometer from ThermoFisher Scientific by using a micro-focus Al-Kα X-ray source (30-400 µm spot size). Data acquisition and processing employing the Thermo Avantage software are described elsewhere.[31] For quantification, the analyzer transmission function, Scofield sensitivity factors, and effective attenuation lengths (EALs) for photoelectrons were applied. EALs were calculated using the standard TPP-2M formalism.[32] All spectra are referenced to the C 1s peak of adventitious carbon at 285.0 eV. CasaXPS software (Casa Software Ltd.) was used to fit the experimental data assuming Voigt profiles with a binding energy uncertainty of ±0.2 eV.

The SSB test cells within the differential electrochemical mass spectrometry (DEMS) setup comprised 100 µm-thick In foil as anode (Alfa Aesar; Ø 8 mm) instead of LTO. Apart from that, the same materials as described above were used. However, assembling was done in a PEEK ring implementable in the DEMS system and allowing relatively high pressures to be applied to the pellet without any cracking occurring. The procedure was conducted by pressing β-Li_3PS_4 SE (110 mg) at 125 MPa, followed by pressing cathode composite (13 mg, ~2.1 mAh cm^{-2}) together with an Al mesh (Ø 8 mm) at 440 MPa. The assembled PEEK ring was then placed in the DEMS system. In addition, a stainless steel mesh (Ø 9 mm) to promote electronic connectivity was placed on top of the Al mesh/cathode layer. The In foil was attached to the other side of the pellet. Contacting the cell was done by stainless steel current collectors, whereby the cathode side included tiny holes to ensure the gases released during operation are able to exit effectively toward the outflow. Electrochemical cycling was performed at 45 °C using a BioLogic VSP-300 potentiostat. To allow the cell to stabilize at this temperature as well as to establish a proper background for the mass spectrometer, a 6 h open circuit voltage (OCV) step was included in the beginning. The cells were then charged/discharged galvanostatically at a C/20 rate in the voltage range between 2.3 and 3.8 V vs In/InLi (~2.9-4.4 V vs Li^+/Li). The flow of He carrier gas was controlled at 2.5 mL min^{-1}. For gas analysis, an OmniStar GSD 320 O2 (Pfeiffer Vacuum GmbH) was used. After each DEMS measurement, a calibration gas was introduced into the mass spectrometer to convert the measured ionic current into a molar value. Further details on the DEMS setup are available in the literature.[25,33]

Results and Discussion

SEM images were taken before and after coating of the NCM622 powder to analyze potential changes in surface morphology. As can be seen in **Figure 1a**, the top surface of the bare NCM622 secondary particles appears rather clean, whereas the presence of a surface shell is evident for both the Li_2CO_3-coated and Li_2CO_3/$LiNbO_3$-coated NCM622 (**Figures 1b** and **1c**). PXRD patterns obtained on the different NCM622 CAMs do not show any reflections of crystalline carbonate and/or niobate species (**Figure S1**). This result may be due to either the amorphous nature of the coating layers or the fact that their fraction is too little to be detected by XRD. From the imaging data and taking into account the SEM-EDX mapping results for the Li_2CO_3/$LiNbO_3$-coated NCM622 in **Figure 1d**-**i**, we conclude that the secondary particles are coated reasonably well.

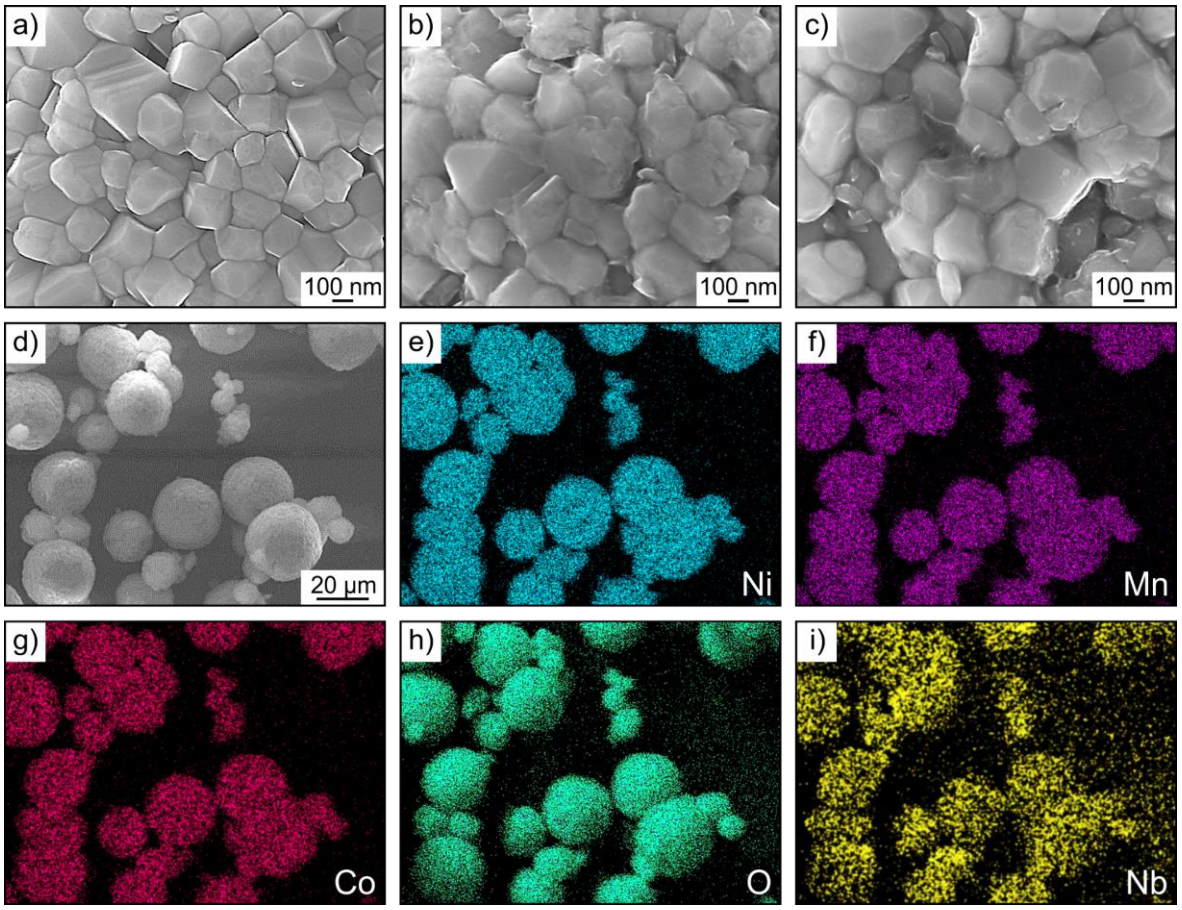

Figure 1. High-magnification SEM images of (a) bare, (b) Li_2CO_3-coated, and (c) Li_2CO_3/$LiNbO_3$-coated NCM622. (d) Low-magnification SEM image of Li_2CO_3/$LiNbO_3$-coated NCM622 and corresponding EDX maps of (e) Ni, (f) Mn, (g) Co, (h) O, and (i) Nb.

To gain more insight into the nature of the surface layers, TEM measurements were conducted on both the Li_2CO_3-coated and Li_2CO_3/$LiNbO_3$-coated NCM622. The high-angle annular dark-field (HAADF) scanning TEM (STEM) image in **Figure 2a** indicates some variation in thickness of the surface shell in the case of Li_2CO_3-coated NCM622, with an approximate maximum thickness of 12 nm. A similar surface morphology is found for the Li_2CO_3/$LiNbO_3$-coated NCM622 (**Figure 2b**; see also **Figure S2** for HAADF STEM images at different magnifications). In addition, incorporation of Nb in the coating layer is verified by EDX mapping (**Figure 2c**), and electron energy loss spectroscopy (EELS) provides indirect evidence for the presence of Li_2CO_3 (**Figure 2d**). Note that the EELS measurements were performed at about –160 °C using a Gatan cryo holder to protect the coating from damage under the electron beam.

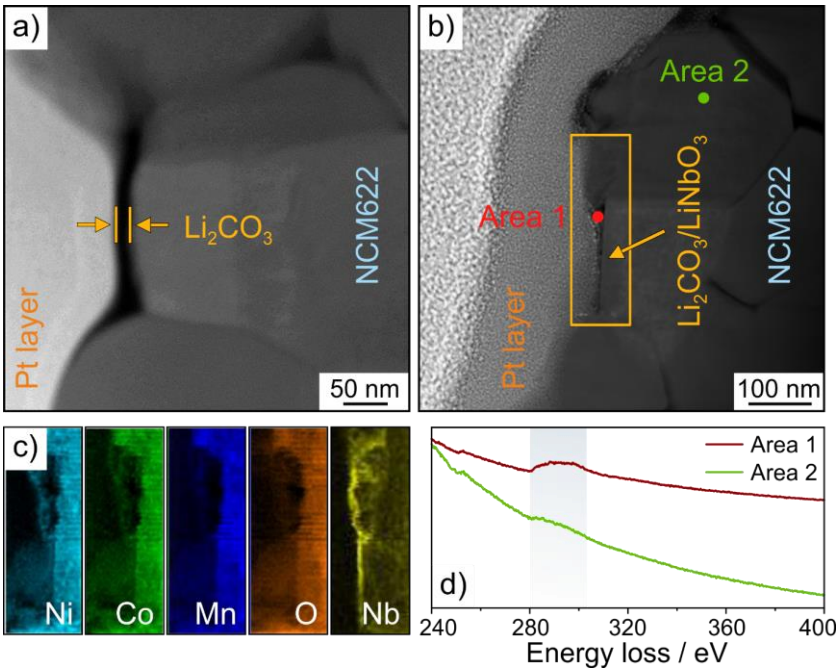

Figure 2. HAADF STEM images of (a) Li_2CO_3-coated and (b) $Li_2CO_3/LiNbO_3$-coated NCM622. (c) EDX maps for the area denoted by the orange box in (b). (d) EEL spectra from the areas denoted in (b), with the C K-edge being highlighted.

The presence of Li_2CO_3 in the relevant coating layers is further corroborated by ATR-IR spectroscopy. For both the Li_2CO_3-coated and $Li_2CO_3/LiNbO_3$-coated NCM622, bands around 1490 and 1430 cm^{-1} (stretching vibrations) and 870 cm^{-1} (in-plane deformation) can be clearly observed (**Figure 3a**), corresponding to IR-active vibrations of the carbonate group.[34] These bands are hardly visible for bare NCM622, indicating minor surface carbonate residuals. In addition, relatively weaker bands around 1170 and 1130 cm^{-1} are found, which seem to be related to the CAM itself.

Next, the Li_2CO_3 content was quantified by acid titration coupled with mass spectrometry (**Figure 3b**). As somewhat expected from the ATR-IR results, bare NCM622 indeed shows the lowest carbonate content (0.11 wt.%), followed by $Li_2CO_3/LiNbO_3$-coated NCM622 (0.65 wt.%) and Li_2CO_3-coated NCM622 (0.84 wt.%). The $LiNbO_3$ content was determined by ICP-OES to be 0.87 wt.% (**Table S1**). Thus, by combining the data from acid titration and ICP-OES, the total content of $Li_2CO_3/LiNbO_3$ coating on NCM622 can be estimated to be 1.52 wt.%.

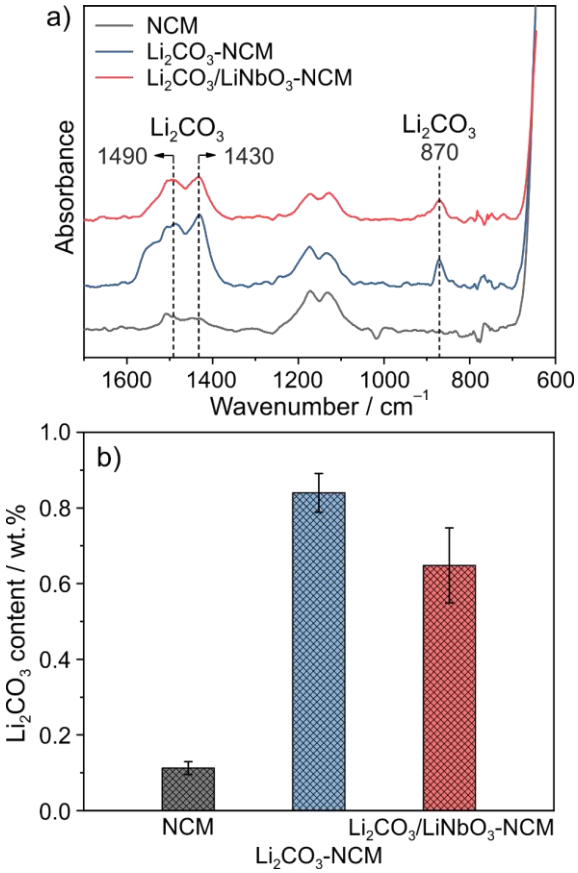

Figure 3. (a) ATR-IR spectra of bare (gray), Li_2CO_3-coated (blue), and $Li_2CO_3/LiNbO_3$-coated NCM622 (red) and (b) corresponding Li_2CO_3 contents from acid titration. Error bars in (b) indicate the standard deviation from two independent measurements.

The electrochemical performance at a C/10 rate and 25 °C of both the Li_2CO_3-coated and $Li_2CO_3/LiNbO_3$-coated NCM622 in pelletized SSB cells using β-Li_3PS_4 SE and LTO anode was tested and compared to that of bare NCM622. **Figure 4a** depict the first and second cycle charge/discharge curves for the different cells, showing the characteristic profile of Ni-rich NCMs (d*q*/d*V* plots in **Figure S3**).[35] Initial specific charge and discharge capacities of 136 and 106 mAh g_{NCM}^{-1} (data are averaged from two independent experiments), respectively, were achieved for the bare NCM622, leading to a first cycle Coulombic efficiency of 78% (**Figure 4b**). If Li_2CO_3 is applied as a coating to the NCM622, the initial specific capacities increase significantly, reaching values of 148 and 124 mAh g_{NCM}^{-1} (84% Coulombic efficiency). Combining both Li_2CO_3 and $LiNbO_3$ leads to a further increase in specific capacities to 157 and 136 mAh g_{NCM}^{-1} and in Coulombic efficiency to 87%. The improvements in the first cycle suggest that the $Li_2CO_3/LiNbO_3$-coated NCM622 exhibits higher surface coverage, in agreement with the total coating content from ICP-OES and acid titration (0.84 vs 1.52 wt.%). In the second cycle, the Coulombic efficiency was found to stabilize around 99% for both the Li_2CO_3-coated and $Li_2CO_3/LiNbO_3$-coated NCM622. In contrast, that of the cell using bare NCM622 was only about 97%, indicating that (severe) side reactions do still occur after the initial cycle. This finding is also reflected in the increase in overvoltage by about 100 mV in the second charge cycle (i.e., sluggish kinetics, probably due to formation of a decomposition layer at the SE/CAM interfaces). Regarding the long-term

cycling performance, the bare NCM622 cell showed virtually linear capacity decay with cycling, leading to 64% capacity retention after 100 cycles (**Figure 4c**). In contrast, 79 and 91% of the initial specific discharge capacity were retained for the Li_2CO_3-coated and Li_2CO_3/$LiNbO_3$-coated NCM622, respectively.

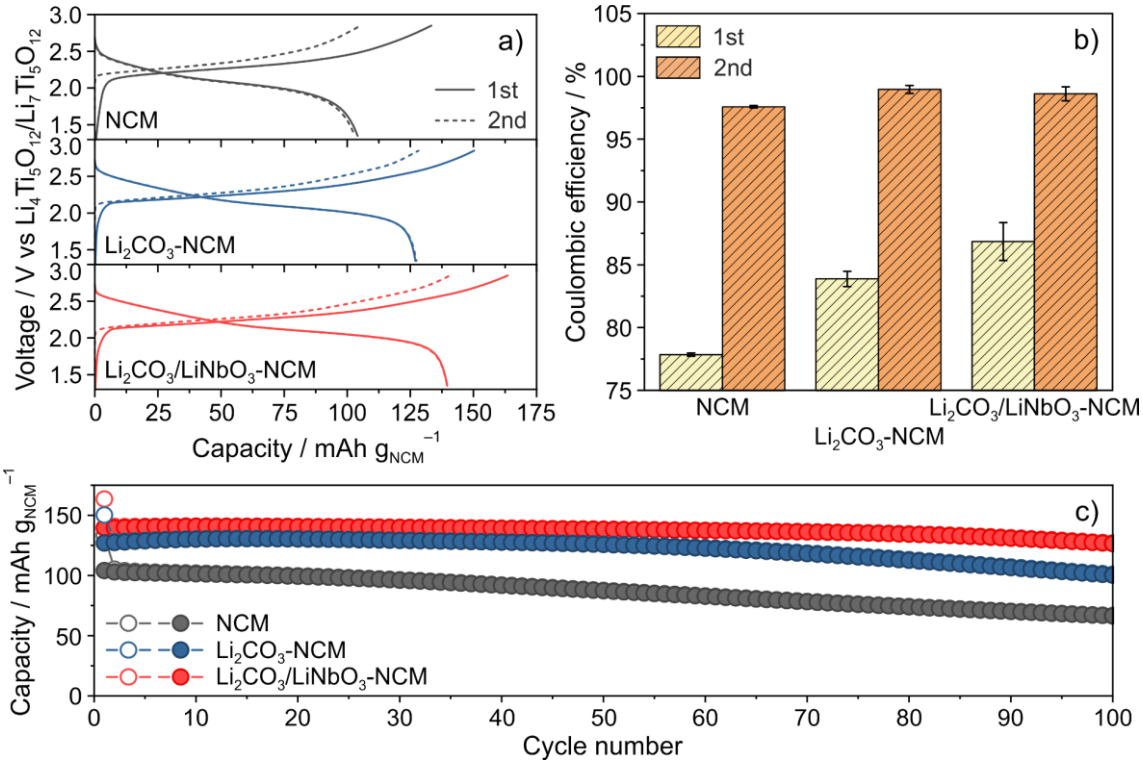

Figure 4. (a) Initial and second cycle voltage profiles, (b) corresponding Coulombic efficiencies, and (c) cycling performance at a C/10 rate and 25 °C of SSB cells using bare (gray), Li_2CO_3-coated (blue), and Li_2CO_3/$LiNbO_3$-coated NCM622 (red). Error bars in (b) indicate the standard deviation from two independent cells.

For better understanding of the performance degradation related to interfacial SE degradation, EIS was conducted on the different SSB cells after 100 cycles. The corresponding Nyquist plots are shown together with the fits in **Figure 5**.[6,8,12] Evidently, the SE bulk resistance (450-500 Ω) is the major component of cell resistance. The SE grain boundary resistance is found to be 40-70 Ω. Note that deviations originate from electrode inhomogeneities and some variation among the cells tested. The interfacial SE/CAM resistance was around 900 Ω in the case of bare NCM622 (**Figure 5a**), compared to only 60 and 25 Ω for the Li_2CO_3-coated and Li_2CO_3/$LiNbO_3$-coated NCM622, respectively (**Figures 5b** and **5c**). Overall, this result is in agreement with the trends seen from electrochemical testing. The fact that the bare NCM622 secondary particles are little protected from direct contact with the β-Li_3PS_4 SE leads to adverse side reactions at the SE/CAM interfaces, and therefore to poor cyclability. However, as for the resistance buildup and cell stability/longevity, it seems that the Li_2CO_3/$LiNbO_3$ coating is superior to the Li_2CO_3-only coating, as the interfacial resistance is about halved for the former.

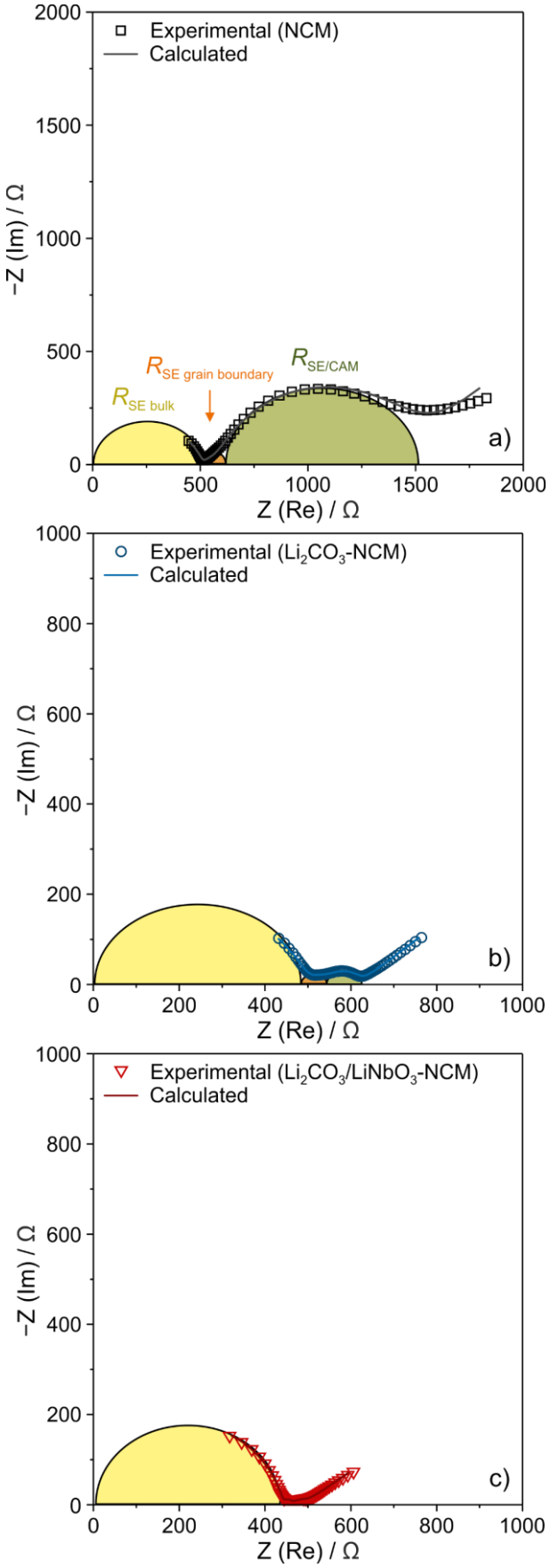

Figure 5. Nyquist plots of SSB cells in the discharged state using (a) bare (gray), (b) Li_2CO_3-coated (blue), and (c) Li_2CO_3/$LiNbO_3$-coated NCM622 (red) after 100 cycles. The semicircles are for eye guidance and depict the resistance contribution from the

bulk SE, SE grain boundary, and SE/CAM interfaces in yellow, orange, and green, respectively.

To gain chemical insights into the side reactions occurring at the SE/CAM interfaces, XPS was conducted on the composite cathodes after 40 cycles. To this end, SSB cells were disassembled in the glovebox and then transferred to the spectrometer without exposure to ambient atmosphere. Particular attention was paid to the S 2p and P 2p core level regions, since it is known that lithium thiophosphates decompose electrochemically to some extent during cycling.[6,36–38] Both the pristine β-Li_3PS_4 SE and the as-prepared composite cathodes were examined first (**Figure S4**). A single doublet with peaks at binding energies of 161.4 ($2p_{3/2}$) and 162.6 eV ($2p_{1/2}$) is found in the S 2p data for all samples, corresponding to the PS_4^{3-} unit. Notably, there is no immediate evidence of a reaction occurring when the NCM622 CAM and β-Li_3PS_4 are mixed together. By comparing the spectra to that obtained after 40 cycles (**Figure 6**), significant S 2p line broadening toward higher binding energy is noticed, hinting at interfacial side reactions. Specifically, new doublets with peaks centered at 162.9 and 163.3 eV and 163.9 and 164.6 eV are found, and their appearance seems indicative of S–S bond formation (i.e., formation of $P_2S_8^{4-}$ and related thiophosphate species [P_2S_x with $x > 5$] and polysulfides/S^0, respectively) due to oxidation of S^{2-}.[6,36,37] These doublets are clearly visible for the Li_2CO_3-coated and Li_2CO_3/$LiNbO_3$-coated NCM622 cathodes, just like for the bare NCM622. This finding thus demonstrates that in line with expectations, there are interparticle junctions between the NCM622 and Li_3PS_4, despite the presence of a surface coating. Moreover, the appearance of a shoulder at lower binding energy is observed in the case of Li_2CO_3-coated NCM622. This new doublet with peaks at 159.9 and 160.8 eV can likely be ascribed to Li_2S.[6,39,40] Because it is only found for the Li_2CO_3-coated NCM622 cathode, we hypothesize that the origin and amount of Li_2S formation are somewhat associated with both the carbonate species present and the carbonate content; however, the reaction pathway remains elusive.

Similar to the S 2p data, a single doublet with peaks centered at 132.0 ($2p_{3/2}$) and 132.9 eV ($2p_{1/2}$) is found in the P 2p spectrum of the pristine β-Li_3PS_4 and the as-prepared composite cathodes (**Figure S4**). After 40 cycles, line broadening toward higher binding energy is observed again for all samples, with the new doublets at binding energies of 132.6/133.0 eV and 133.7/134.4 eV being characteristic of P–S–P and P–O bond formation, respectively.[36,39,41] The presence of P_xO_y species may be due to reaction of the β-Li_3PS_4 SE with gases evolving during electrochemical cycling (see section on DEMS below).[25]

Taken together, XPS clearly demonstrates that sulfur oxidation occurs during cycling, irrespective of the surface modification of NCM622. However, the as-formed interfacial layer (clearly impeding charge transfer across the SE/CAM interfaces) most likely differs in thickness among the composite cathodes tested. Based on the above results, it seems reasonable to assume that this layer is much thicker for bare than the Li_2CO_3-coated and Li_2CO_3/$LiNbO_3$-coated NCM622, helping to explain the superior electrochemical performance of the latter materials. However, the open question

remains as to why the use of Li_2CO_3-only coating results in some performance decline compared to the Li_2CO_3/$LiNbO_3$ coating.

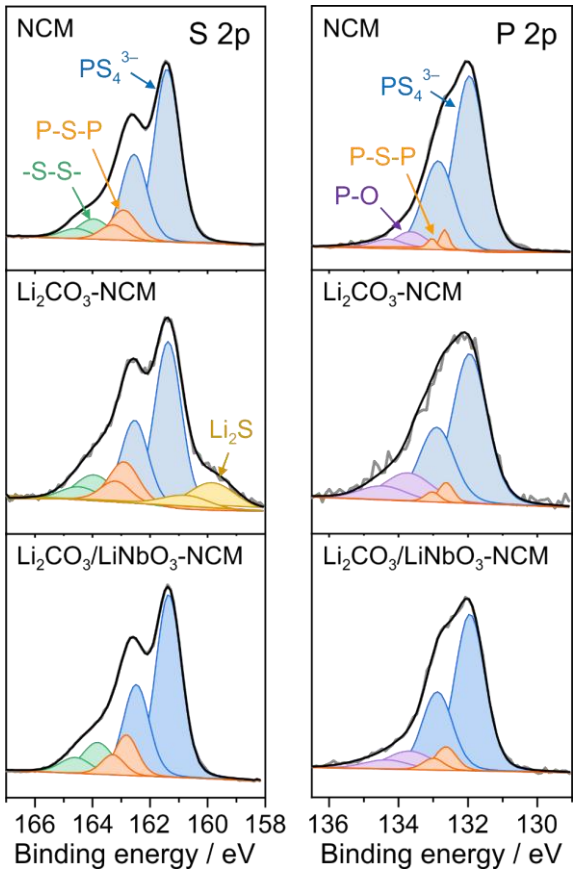

Figure 6. Detailed XPS spectra of S 2p and P 2p core level regions for composite cathodes using bare, Li_2CO_3-coated, and Li_2CO_3/$LiNbO_3$-coated NCM622 after 40 cycles. Gray and black lines represent the experimental data and fitting results, respectively.

Now having shown the beneficial effect of the surface coatings on the electrochemical performance and rationalized the findings *via* EIS and XPS, the intriguing question arises if the incorporated carbonate species lead to CO_2 gas evolution during cycling, and thus have an additional influence on the SE/CAM interfaces.[25] To analyze this, SSB cells compromising either the Li_2CO_3-coated or Li_2CO_3/$LiNbO_3$-coated NCM622 were cycled in a custom DEMS setup in the same voltage window applied for the long-term cycling tests (~2.9-4.4 V vs Li^+/Li) while simultaneously monitoring gas evolution (mass signals from m/z = 1 to 100). As depicted in **Figure 7a** and in agreement with the data in **Figure 4**, the Li_2CO_3-coated NCM622 cell showed a lower performance in the first cycle (q_{ch} ≈ 126 mAh g_{NCM}^{-1}, compared to 142 mAh g_{NCM}^{-1} for the Li_2CO_3/$LiNbO_3$-coated NCM622 cell). Regarding the m/z = 44 signal (CO_2), sharp peaks are observed right at the beginning of the initial charge cycle (**Figure 7b**). Such CO_2 release also occurs in LIBs and is typically attributed to the electrochemical reduction of carbonate species (liquid electrolyte) at the anode side. However, this explanation can be excluded here. So far, the origin of CO_2 evolution in SSB cells (with the beginning of charging) remains elusive and further studies are currently in progress.

In the further course, broad, relatively symmetric peaks appear for both the Li_2CO_3-coated and Li_2CO_3/$LiNbO_3$-coated NCM622 with an onset potential around 3.6 V vs In/InLi (equivalent to ~4.2 V vs Li^+/Li; **Figure S5**) and maximum amplitude at the upper cutoff potential (**Figure 7b**). This observation can be attributed to the electrochemical decomposition of Li_2CO_3, leading to CO_2 and $^1O_2$ formation.[42] The amount of CO_2 formed per gram of NCM622 is higher by a factor of approximately six for the Li_2CO_3-coated NCM622 (2400 vs 430 nmol g_{NCM}^{-1}), despite the fact that the carbonate content from acid titration is comparable for both samples. This result strongly implies the Li_2CO_3/$LiNbO_3$ layer to be a hybrid or solid solution coating rather than separated fractions of Li_2CO_3 along with $LiNbO_3$.

In recent years, it has been reported that electrochemical decomposition of Li_2CO_3 liberates CO_2 among highly reactive singlet oxygen, which is prone to react with liquid carbonate-based organic electrolytes, thereby forming CO_2.[26] In a recent publication, we have shown that such correlation can most likely be transferred to lithium thiophosphate systems, where the formed $^1O_2$ reacts with the SE to produce highly corrosive SO_2.[25] Hence, the question arises if such SO_2 release can also be monitored for the coated NCM622 samples discussed herein. As illustrated in **Figure 7c**, no O_2 evolution (*m*/*z* = 32) was detectable, independent of the coating chemistry. Consequently, either the amount of released O_2 was just beyond the detection limit of the system or the possibly formed O_2 underwent a reaction with the SE. Following this line, for the Li_2CO_3-coated NCM622, an increased mass signal *m*/*z* = 64, corresponding to SO_2, was observed (**Figure 7d**). In contrast, for the Li_2CO_3/$LiNbO_3$-coated NCM622, no such SO_2 evolution was detected, in agreement with the six times smaller amount of released CO_2. Also, the onset potentials of both CO_2 and SO_2 evolution consistently occur at around 3.6 V vs In/InLi for the initial and subsequent cycles (**Figure S6**). This result leads us to the conclusion that surface carbonate decomposition indeed results in the release of highly reactive $^1O_2$, which further reacts with the β-Li_3PS_4 to form SO_2. Note that the upper cutoff potential applied (and the corresponding state of charge) is well below the limit of oxygen release from the NCM622 lattice.[25,43] Also, as expected, only minor CO_2 evolution (comparable to the Li_2CO_3/$LiNbO_3$-coated NCM622 cell) was observed for the bare NCM622 (**Figure S7**), underlining the stabilizing effect of the hybrid coating.

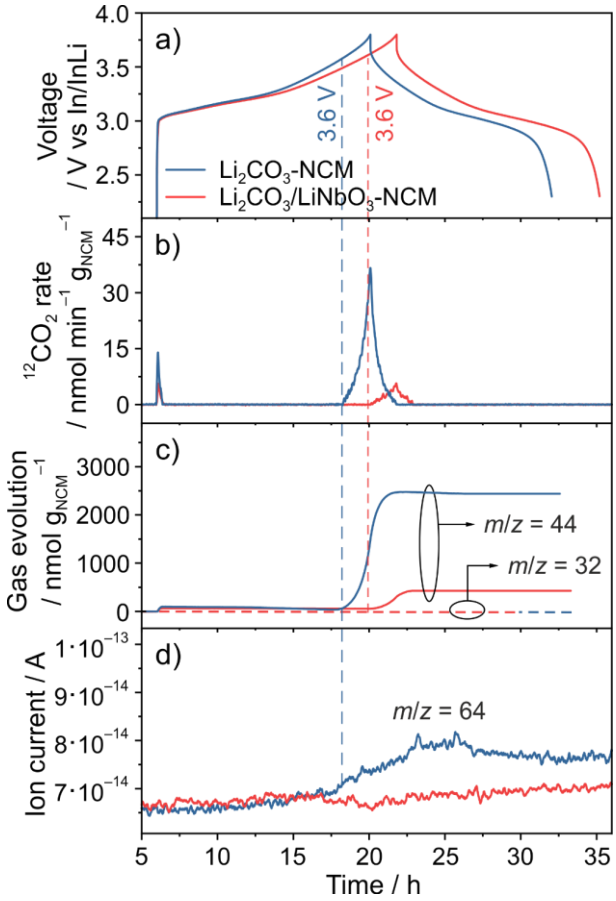

Figure 7. (a) First cycle voltage profile at a C/20 rate and 45 °C of SSB cells using Li_2CO_3-coated (blue) and Li_2CO_3/$LiNbO_3$-coated NCM622 (red). The CO_2 mass signals (*m*/*z* = 44) are shown in (b) and the cumulative amounts are depicted in (c). (d) Time-resolved ion current for SO_2 evolution (*m*/*z* = 64).

Finally, top view and cross-sectional SEM images of the composite electrodes after 100 cycles were taken to visualize any possible effects of SE decomposition on the cathode morphology and microstructure. As can be seen from **Figure 8a**, the micron-size (spherical) NCM622 secondary particles can be clearly distinguished from the β-Li_3PS_4 SE. In the case of bare NCM622, distinct changes in surface and bulk morphology are observed after cycling (**Figures 8b** and **S8**). The SE decomposition is so pronounced that individual particles are hardly visible anymore. Instead, a thick decomposition layer (reminiscent of amorphous material) has formed at the SE/CAM interfaces throughout the electrode. For the Li_2CO_3-coated NCM622, similar changes in SE appearance are observed (**Figure 8c**), however, to a lesser extent compared to bare NCM622. Interestingly, such apparent SE decomposition is not visible from the SEM imaging data for the Li_2CO_3/$LiNbO_3$-coated NCM622 (**Figure 8d**). In fact, the initial electrode morphology and structure are largely preserved (see also **Figure S8**), thus indirectly emphasizing that the SE/CAM interfaces are reasonably robust (in terms of stability). Note that SE amorphization could not be monitored by XRD, as the NCM622 is much more crystalline and the corresponding reflections are more intense compared to the β-Li_3PS_4.

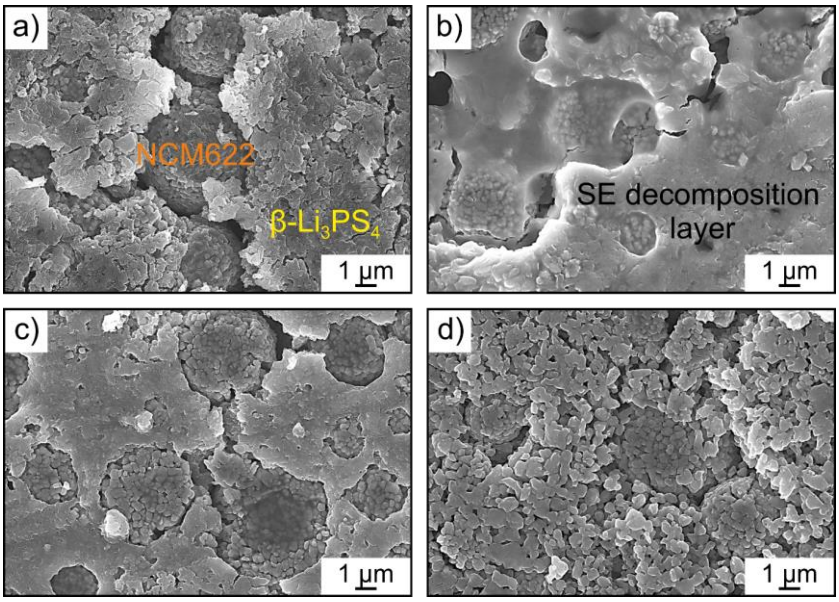

Figure 8. Top view SEM images of composite cathodes (a) before and (b-d) after 100 cycles: (a, d) Li_2CO_3/$LiNbO_3$-coated, (b) bare, and (c) Li_2CO_3-coated NCM622.

From the above data, it is clear that interfacial SE decomposition is indeed strongly dependent on the coating chemistry (**Figure 9**). For bare NCM622, severe SE degradation occurs, eventually leading to large interfacial resistance (impedance buildup with cycling) and significant capacity fading, as already observed by others.[6,37] However, the cycling performance and stability can be improved considerably by simply increasing the amount of carbonate species on the top surface of the NCM622 secondary particles. Additional incorporation of $LiNbO_3$ to form a hybrid or solid solution coating leads to a further increase in performance. As evidenced by DEMS, this boost is due to improvements in (electrochemical) stability of the coating layer, among others.

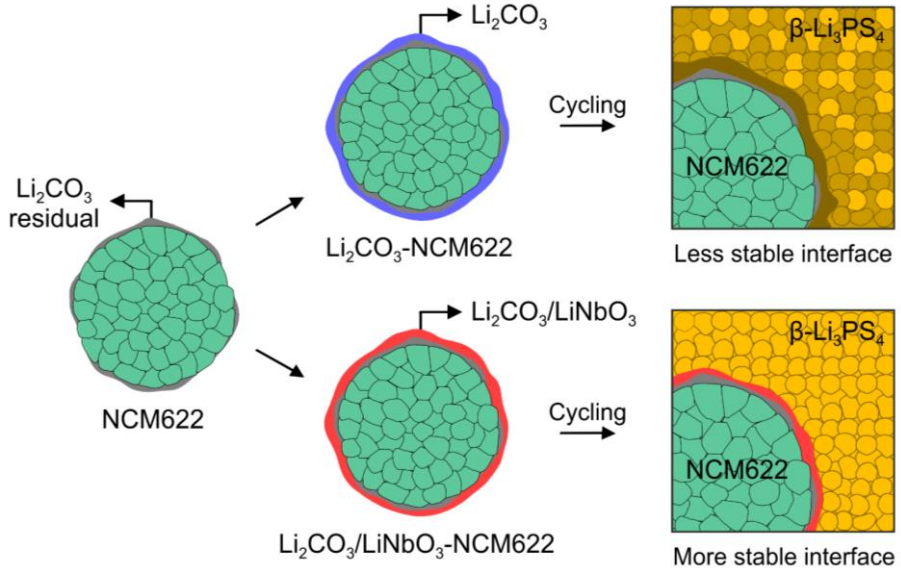

Figure 9. Illustration of the different interfacial reactivity when using the Li_2CO_3-coated (indicated by SE oxidation in dark brown) or Li_2CO_3/$LiNbO_3$-coated NCM622 in β-

Li_3PS_4-based SSB cells. Reasonably stable SE/CAM interfaces are achieved only for the Li_2CO_3/$LiNbO_3$ hybrid coating.

Conclusions

In summary, we have studied in this work the effect of Li_2CO_3 coatings on Ni-rich layered oxide cathode material (NCM622) on the cyclability of all-solid-state battery cells using β-Li_3PS_4 as solid electrolyte. Our results show that surface carbonate species indeed help to improve the performance significantly (compared to uncoated NCM622), albeit capacity fading still occurs. Incorporation of sol-gel-derived $LiNbO_3$, and thereby formation of a Li_2CO_3/$LiNbO_3$ hybrid coating, possibly a solid solution coating, results in an additional increase in performance (compared to Li_2CO_3-coated NCM622). These findings are confirmed by complementary techniques, including electrochemical impedance and X-ray photoelectron spectroscopy, differential electrochemical mass spectrometry, and electron microscopy analysis, indicating that more stable interfaces are formed in composite cathodes using the Li_2CO_3/$LiNbO_3$-coated NCM622. We also demonstrate that while the carbonate content is similar for both the Li_2CO_3-coated and Li_2CO_3/$LiNbO_3$-coated NCM622, the former material shows significantly more CO_2 evolution, due to decomposition of the relevant carbonate species during cycling, and therefore SO_2 formation. However, there are still open questions to be addressed regarding the optimal carbonate content as well as the prevailing chemical and phase composition and the corresponding properties (stability, conductivity, etc.) of the coating layer.

In a broader context, our results provide evidence for the beneficial effect of carbonate-containing ternary oxide coatings in achieving stable performance of Ni-rich NCM cathodes in all-solid-state battery cells. They also emphasize the significance of taking surface contaminants and gas evolution into account in designing coatings with tailored properties. Such considerations will become even more important when NCM cathode materials with >60% Ni are used (note that these materials are much more prone to surface Li_2CO_3 formation during synthesis and storage), like in conventional high-energy-density Li-ion batteries.

Associated Content

The Supporting Information is available free of charge on the ACS Publications website. PXRD patterns; elemental composition from ICP-OES and acid titration; d*q*/d*V* plots of the initial cycle; S 2p and P 2p XPS spectra before cycling; additional DEMS and electron microscopy imaging data.

Author Information

Corresponding Authors

*Phone: +49 721 60828051; E-mail: a-young.kim@kit.edu

*Phone: +49 721 60828907; E-mail: florian.strauss@kit.edu

*Phone: +49 721 60828827; E-mail: torsten.brezesinski@kit.edu

ORCID

A-Young Kim: 0000-0001-6124-0807

Florian Strauss: 0000-0001-5817-6349

Jun Hao Teo: 0000-0002-0343-669X

Toru Hatsukade: 0000-0001-9016-0929

Andrey Mazilkin: 0000-0001-7805-8526

Jürgen Janek: 0000-0002-9221-4756

Torsten Brezesinski: 0000-0002-4336-263X

Notes

The authors declare no competing financial interest.

Acknowledgments

This study is part of the projects being funded within the BASF International Network for Batteries and Electrochemistry. This work was partly carried out with the support of the Karlsruhe Nano Micro Facility (KNMF, www.knmf.kit.edu), a Helmholtz Research Infrastructure at Karlsruhe Institute of Technology (KIT, www.kit.edu). T. Bartsch and J. H. Teo thank the German Federal Ministry of Education and Research (BMBF) for funding within the project ARTEMYS (03XP0114J). The authors thank Thomas Bergfeldt for ICP-OES, Dominic Boll for XPS, and Christian Grupe for graphical assistance.

References

(1) Tarascon, J.-M.; Armand, M. Issues and Challenges Facing Rechargeable Lithium Batteries. *Nature* **2001**, *414*, 359.

(2) Thackeray, M. M.; Wolverton, C.; Isaacs, E. D. Electrical Energy Storage for Transportation—Approaching the Limits Of, and Going Beyond, Lithium-Ion Batteries. *Energy Environ. Sci.* **2012**, *5*, 7854–7863.

(3) Larcher, D.; Tarascon, J.-M. Towards Greener and More Sustainable Batteries for Electrical Energy Storage. *Nat. Chem.* **2015**, *7*, 19–29.

(4) Janek, J.; Zeier, W. G. A Solid Future for Battery Development. *Nat. Energy* **2016**, *1*, 16141.

(5) Kato, Y.; Hori, S.; Saito, T.; Suzuki, K.; Hirayama, M.; Mitsui, A.; Yonemura, M.; Iba, H.; Kanno, R. High-Power All-Solid-State Batteries Using Sulfide Superionic Conductors. *Nat. Energy* **2016**, *1*, 16030.

(6) Koerver, R.; Aygün, I.; Leichtweiß, T.; Dietrich, C.; Zhang, W.; Binder, J. O.; Hartmann, P.; Zeier, W. G.; Janek, J. Capacity Fade in Solid-State Batteries: Interphase Formation and Chemomechanical Processes in Nickel-Rich Layered Oxide Cathodes and Lithium Thiophosphate Solid Electrolytes. *Chem. Mater.* **2017**, *29*, 5574–5582.

(7) Haruyama, J.; Sodeyama, K.; Han, L.; Takada, K.; Tateyama, Y. Space–charge Layer Effect at Interface between Oxide Cathode and Sulfide Electrolyte in All-Solid-State Lithium-Ion Battery. *Chem. Mater.* **2014**, *26*, 4248–4255.
(8) Ohta, N.; Takada, K.; Zhang, L.; Ma, R.; Osada, M.; Sasaki, T. Enhancement of the High-Rate Capability of Solid-State Lithium Batteries by Nanoscale Interfacial Modification. *Adv. Mater.* **2006**, *18*, 2226–2229.
(9) Culver, S. P.; Koerver, R.; Zeier, W. G.; Janek, J. On the Functionality of Coatings for Cathode Active Materials in Thiophosphate-Based All-Solid-State Batteries. *Adv. Energy Mater.* **2019**, *9*, 1900626.
(10) Ohta, N.; Takada, K.; Sakaguchi, I.; Zhang, L.; Ma, R.; Fukuda, K.; Osada, M.; Sasaki, T. $LiNbO_3$-Coated $LiCoO_2$ as Cathode Material for All Solid-State Lithium Secondary Batteries. *Electrochem. Commun.* **2007**, *9*, 1486–1490.
(11) Takada, K.; Ohta, N.; Zhang, L.; Fukuda, K.; Sakaguchi, I.; Ma, R.; Osada, M.; Sasaki, T. Interfacial Modification for High-Power Solid-State Lithium Batteries. *Solid State Ion.* **2008**, *179*, 1333–1337.
(12) Okada, K.; Machida, N.; Naito, M.; Shigematsu, T.; Ito, S.; Fujiki, S.; Nakano, M.; Aihara, Y. Preparation and Electrochemical Properties of $LiAlO_2$-Coated $Li(Ni_{1/3}Mn_{1/3}Co_{1/3})O_2$ for All-Solid-State Batteries. *Solid State Ion.* **2014**, *255*, 120–127.
(13) Ito, S.; Fujiki, S.; Yamada, T.; Aihara, Y.; Park, Y.; Kim, T. Y.; Baek, S.-W.; Lee, J.-M.; Doo, S.; Machida, N. A Rocking Chair Type All-Solid-State Lithium Ion Battery Adopting Li_2O–ZrO_2 Coated $LiNi_{0.8}Co_{0.15}Al0_{.05}O_2$ and a Sulfide Based Electrolyte. *J. Power Sources* **2014**, *248*, 943–950.
(14) Wang, C.; Chen, L.; Zhang, H.; Yang, Y.; Wang, F.; Yin, F.; Yang, G. Li_2ZrO_3 Coated $LiNi_{1/3}Co_{1/3}Mn_{1/3}O_2$ for High Performance Cathode Material in Lithium Batteries. *Electrochimica Acta* **2014**, *119*, 236–242.
(15) Seki, S.; Kobayashi, Y.; Miyashiro, H.; Mita, Y.; Iwahori, T. Fabrication of High-Voltage, High-Capacity All-Solid-State Lithium Polymer Secondary Batteries by Application of the Polymer Electrolyte/Inorganic Electrolyte Composite Concept. *Chem. Mater.* **2005**, *17*, 2041–2045.
(16) Jung, S. H.; Oh, K.; Nam, Y. J.; Oh, D. Y.; Brüner, P.; Kang, K.; Jung, Y. S. Li_3BO_3–Li_2CO_3: Rationally Designed Buffering Phase for Sulfide All-Solid-State Li-Ion Batteries. *Chem. Mater.* **2018**, *30*, 8190–8200.
(17) Sakuda, A.; Kitaura, H.; Hayashi, A.; Tadanaga, K.; Tatsumisago, M. Modification of Interface between $LiCoO_2$ Electrode and Li_2S–P_2S_5 Solid Electrolyte Using Li_2O–SiO_2 Glassy Layers. *J. Electrochem. Soc.* **2009**, *156*, A27–A32.
(18) Kim, J.; Kim, O.; Park, C.; Lee, G.; Shin, D. Electrochemical Properties of $Li_{1+x}CoO_2$ Synthesized for All-Solid-State Lithium Ion Batteries with Li_2S-P_2S_5 Glass-Ceramics Electrolyte. *J. Electrochem. Soc.* **2015**, *162*, A1041–A1045.
(19) Kim, J.; Kim, M.; Noh, S.; Lee, G.; Shin, D. Enhanced Electrochemical Performance of Surface Modified $LiCoO_2$ for All-Solid-State Lithium Batteries. *Ceram. Int.* **2016**, *42*, 2140–2146.
(20) Heitjans, P.; Masoud, M.; Feldhoff, A.; Wilkening, M. NMR and Impedance Studies of Nanocrystalline and Amorphous Ion Conductors: Lithium Niobate as a Model System. *Faraday Discuss.* **2007**, *134*, 67–82.

(21) Kim, D. H.; Oh, D. Y.; Park, K. H.; Choi, Y. E.; Nam, Y. J.; Lee, H. A.; Lee, S.-M.; Jung, Y. S. Infiltration of Solution-Processable Solid Electrolytes into Conventional Li-Ion-Battery Electrodes for All-Solid-State Li-Ion Batteries. *Nano Lett.* **2017**, *17*, 3013–3020.
(22) Jung, R.; Morasch, R.; Karayaylali, P.; Phillips, K.; Maglia, F.; Stinner, C.; Shao-Horn, Y.; Gasteiger, H. A. Effect of Ambient Storage on the Degradation of Ni-Rich Positive Electrode Materials (NMC811) for Li-Ion Batteries. *J. Electrochem. Soc.* **2018**, *165*, A132–A141.
(23) Kim, J.; Hong, Y.; Ryu, K. S.; Kim, M. G.; Cho, J. Washing Effect of a $LiNi_{0.83}Co_{0.15}Al_{0.02}O_2$ Cathode in Water. *Electrochem. Solid-State Lett.* **2006**, *9*, A19–A23.
(24) Renfrew, S. E.; McCloskey, B. D. Residual Lithium Carbonate Predominantly Accounts for First Cycle CO_2 and CO Outgassing of Li-Stoichiometric and Li-Rich Layered Transition-Metal Oxides. *J. Am. Chem. Soc.* **2017**, *139*, 17853–17860.
(25) Bartsch, T.; Strauss, F.; Hatsukade, T.; Schiele, A.; Kim, A.-Y.; Hartmann, P.; Janek, J.; Brezesinski, T. Gas Evolution in All-Solid-State Battery Cells. *ACS Energy Lett.* **2018**, *3*, 2539–2543.
(26) Hatsukade, T.; Schiele, A.; Hartmann, P.; Brezesinski, T.; Janek, J. Origin of Carbon Dioxide Evolved during Cycling of Nickel-Rich Layered NCM Cathodes. *ACS Appl. Mater. Interfaces* **2018**, *10*, 38892–38899.
(27) Li, L.; Xu, M.; Yao, Q.; Chen, Z.; Song, L.; Zhang, Z.; Gao, C.; Wang, P.; Yu, Z.; Lai, Y. Alleviating Surface Degradation of Nickel-Rich Layered Oxide Cathode Material by Encapsulating with Nanoscale Li-Ions/Electrons Superionic Conductors Hybrid Membrane for Advanced Li-Ion Batteries. *ACS Appl. Mater. Interfaces* **2016**, *8*, 30879–30889.
(28) Strauss, F.; Bartsch, T.; de Biasi, L.; Kim, A.-Y.; Janek, J.; Hartmann, P.; Brezesinski, T. Impact of Cathode Material Particle Size on the Capacity of Bulk-Type All-Solid-State Batteries. *ACS Energy Lett.* **2018**, *3*, 992–996.
(29) Bartsch, T.; Kim, A.-Y.; Strauss, F.; de Biasi, L.; Teo, J. H.; Janek, J.; Hartmann, P.; Brezesinski, T. Indirect State-of-Charge Determination of All-Solid-State Battery Cells by X-ray Diffraction. *Chem. Commun.* **2019**, *55*, 11223–11226.
(30) Zhang, W.; Schröder, D.; Arlt, T.; Manke, I.; Koerver, R.; Pinedo, R.; Weber, D. A.; Sann, J.; Zeier, W. G.; Janek, J. (Electro)chemical Expansion during Cycling: Monitoring the Pressure Changes in Operating Solid-State Lithium Batteries. *J. Mater. Chem. A* **2017**, *5*, 9929–9936.
(31) Parry, K. L.; Shard, A. G.; Short, R. D.; White, R. G.; Whittle, J. D.; Wright, A. ARXPS Characterisation of Plasma Polymerised Surface Chemical Gradients. *Surf. Interface Anal.* **2006**, *38*, 1497–1504.
(32) Tanuma, S.; Powell, C. J.; Penn, D. R. Calculations of Electron Inelastic Mean Free Paths. V. Data for 14 Organic Compounds over the 50–2000 eV Range. *Surf. Interface Anal.* **1994**, *21*, 165–176.
(33) Berkes, B. B.; Jozwiuk, A.; Vračar, M.; Sommer, H.; Brezesinski, T.; Janek, J. Online Continuous Flow Differential Electrochemical Mass Spectrometry with a Realistic Battery Setup for High-Precision, Long-Term Cycling Tests. *Anal. Chem.* **2015**, *87*, 5878–5883.

(34) Busca, G.; Lorenzelli, V. Infrared Spectroscopic Identification of Species Arising from Reactive Adsorption of Carbon Oxides on Metal Oxide Surfaces. *Mater. Chem.* **1982**, *7*, 89–126.
(35) de Biasi, L.; Kondrakov, A. O.; Geßwein, H.; Brezesinski, T.; Hartmann, P.; Janek, J. Between Scylla and Charybdis: Balancing Among Structural Stability and Energy Density of Layered NCM Cathode Materials for Advanced Lithium-Ion Batteries. *J. Phys. Chem. C* **2017**, *121*, 26163–26171.
(36) Auvergniot, J.; Cassel, A.; Foix, D.; Viallet, V.; Seznec, V.; Dedryvère, R. Redox Activity of Argyrodite Li_6PS_5Cl Electrolyte in All-Solid-State Li-Ion Battery: An XPS Study. *Solid State Ion.* **2017**, *300*, 78–85.
(37) Auvergniot, J.; Cassel, A.; Ledeuil, J.-B.; Viallet, V.; Seznec, V.; Dedryvère, R. Interface Stability of Argyrodite Li_6PS_5Cl toward $LiCoO_2$, $LiNi_{1/3}Co_{1/3}Mn_{1/3}O_2$, and $LiMn_2O_4$ in Bulk All-Solid-State Batteries. *Chem. Mater.* **2017**, *29*, 3883–3890.
(38) Chen, H. M.; Maohua, C.; Adams, S. Stability and Ionic Mobility in Argyrodite-Related Lithium-Ion Solid Electrolytes. *Phys. Chem. Chem. Phys.* **2015**, *17*, 16494–16506.
(39) Sang, L.; Haasch, R. T.; Gewirth, A. A.; Nuzzo, R. G. Evolution at the Solid Electrolyte/Gold Electrode Interface during Lithium Deposition and Stripping. *Chem. Mater.* **2017**, *29*, 3029–3037.
(40) Wenzel, S.; Randau, S.; Leichtweiß, T.; Weber, D. A.; Sann, J.; Zeier, W. G.; Janek, J. Direct Observation of the Interfacial Instability of the Fast Ionic Conductor $Li_{10}GeP_2S_{12}$ at the Lithium Metal Anode. *Chem. Mater.* **2016**, *28*, 2400–2407.
(41) Koerver, R.; Walther, F.; Aygün, I.; Sann, J.; Dietrich, C.; Zeier, W. G.; Janek, J. Redox-Active Cathode Interphases in Solid-State Batteries. *J. Mater. Chem. A* **2017**, *5*, 22750–22760.
(42) Mahne, N.; Renfrew, S. E.; McCloskey, B. D.; Freunberger, S. A. Electrochemical Oxidation of Lithium Carbonate Generates Singlet Oxygen. *Angew. Chem. Int. Ed.* **2018**, *57*, 5529–5533.
(43) Jung, R.; Strobl, P.; Maglia, F.; Stinner, C.; Gasteiger, H. A. Temperature Dependence of Oxygen Release from $LiNi_{0.6}Mn_{0.2}Co_{0.2}O_2$ (NMC622) Cathode Materials for Li-Ion Batteries. *J. Electrochem. Soc.* **2018**, *165*, A2869–A2879.